Formation of Rigid Organic Nanotubes with Controlled Internal Cavity Based on Frustrated Aggregate Internal Rearrangement Mechanism

ARTICLE *in* THE JOURNAL OF PHYSICAL CHEMISTRY B · MAY 2013

Impact Factor: 3.3 · DOI: 10.1021/jp4015564 · Source: PubMed

3 AUTHORS, INCLUDING:

Minwoo Han
University of Southern Denmark
8 PUBLICATIONS **35** CITATIONS
SEE PROFILE

Eunji Sim
Yonsei University
62 PUBLICATIONS **849** CITATIONS
SEE PROFILE

THE JOURNAL OF PHYSICAL CHEMISTRY B

Article

pubs.acs.org/JPCB

Formation of Rigid Organic Nanotubes with Controlled Internal Cavity Based on Frustrated Aggregate Internal Rearrangement Mechanism

Minwoo Han, Jungin Hyun, and Eunji Sim*

Department of Chemistry and Institute of Nano-Bio Molecular Assemblies, Yonsei University, 50 Yonsei-ro Seodaemun-gu, Seoul 120-749, Korea

ABSTRACT: We introduce frustrated aggregate internal rearrangement (FAIR) mechanism for anisotropic higher-order structure formations, in which the anisotropy arose due to the structural frustration. We demonstrate the FAIR mechanism by investigating the recently observed rigid organic nanotube formations through the self-assembly of building blocks, which include rigid segments and make intermolecular H-bonds, whereas the principle of the FAIR mechanism is general and is not limited to H-bonding building blocks or nanotube formations. Initially, molecules aggregate into sheetlike structures driven by nonspecific and nondirectional intermolecular interactions such as $\pi-\pi$ stacking or amphiphilicity. Weak intermolecular H-bonds provide additional stability to the structure. Within the aggregate, however, not all molecules have the right orientation for specific and directional H-bonds whereas collective internal rearrangement of rigid building blocks requires a large amount of energy to overcome kinetically trapped barriers. Consequently, instead of the fully H-bonded global equilibrium structure, self-assembled layers become trapped with partial and disordered H-bonding schemes at various fractions leading to an anisotropic layer that undergoes spontaneous transformation into curved structures. The FAIR mechanism can readily be extended to anisotropic higher-order structures other than nanotubes and to the assembly of diverse building blocks including hybrids such as polymer nanocomposites. Also the reversible transformation from metastable nanotubes into layered sheets is potentially useful for controlling internal cavity size of nanotubes.

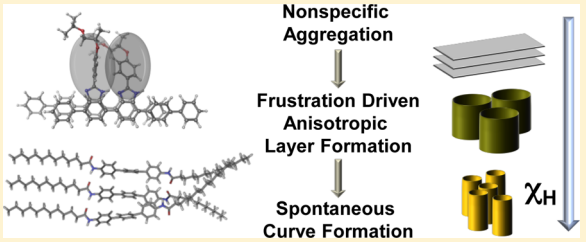

I. INTRODUCTION

Nanoscale structures such as tubes[1−5] and networks[5−7] are higher-order packing materials whose structural complexity has unique chemical and physical properties.[8] In particular, structures with internal cavity are of great interest for potential applications in nano- and biotechnologies as storages,[9,10] channels,[11] drug delivery vehicles,[12] etc. Despite their significance and applicability, organic nanotubes are relatively rare. Most of the organic tubes made of phospholipids, amphiphiles, and peptides are soft,[13] whereas the rigidity of tube structures is crucial for their applications. In recent literature, scroll-like structures were formed through the self-assembly of various building blocks such as rod−coil molecules and cyclic complexes. While molecular shape and type of interactions differ, these building blocks commonly include rigid segments and have intermolecular H-bonding sites.[1−4] Because rigid molecules are bound by the directional H-bonds, the resultant organic tubes are structurally robust. Therefore, understanding the formation mechanism of these nanotubes is of significant importance to shed light on the rigid organic nanotube synthesis and applications. However, the underlying mechanism, especially the role of H-bonds, is still unknown.

Addition of H-bonds into molecular aggregates results in complex self-organized structures: nanofiber networks,[14] superhelical arrangements,[15] and wall- or sheetlike structures[16] are formed depending on the H-bonding sites. Structural characteristics of such higher-order architectures are well understood based on the atom specificity and directionality of H-bonds. On the contrary, the conventional knowledge about the H-bonding scheme is insufficient to explain formation mechanism of the organic nanotubes. In addition, layer structures were observed as a precursor so that preformed layers were seen to undergo spontaneous transformation into curved structures.[1,2] In solution phase, the dominant structure depends on concentration: layered sheets are preferentially formed at high concentrations whereas nanotubes and vesicles are dominant in dilute solutions.[2,3] Two-dimensional (2D) anisotropic sheets have been known to spontaneously transform into various curved phases.[17−20] Hence, the rigid organic nanotubes should be closely associated with anisotropic layer formation for which H-bonds are anticipated to play a role.

In this work, we propose the frustrated aggregate internal rearrangement (FAIR) mechanism for anisotropic higher-order structures. In the presence of conflicting intermolecular forces, simultaneous minimization of interaction energies is prohibited, causing the geometrical frustration.[21] Therefore, the molecular configuration adapts an ensemble of kinetically trapped local equilibrium structures that are anisotropic overall. Subse-

Received: February 13, 2013
Revised: May 2, 2013
Published: May 17, 2013

Scheme 1. Molecular Structures of (a) T-GRC, (b) H-GRC,[1] and (c) L-GRC[2]

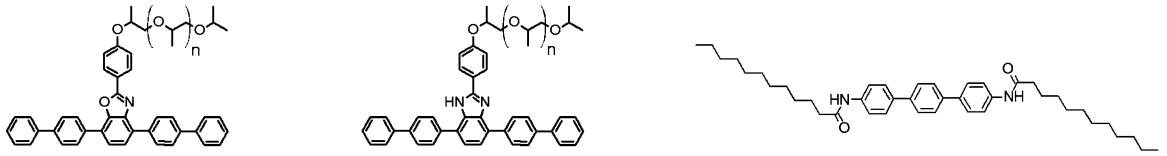

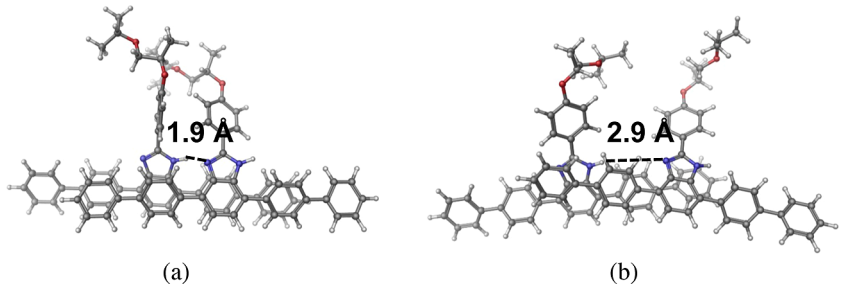

Figure 1. Snapshots of optimized (a) H-bonded geometry (H orientation) and (b) coil-separation constrained geometry (X orientation) of H-GRC[n = 2] in diethyl ether.

quently, the structural anisotropy gives rise to unique and complex higher-order architecture. To demonstrate the FAIR mechanism and to elucidate the new role of H-bonds underlying the anisotropic layer and subsequent nanotube formation, in section II, two independent experimental systems are investigated using density functional theory. Also, in section III, dissipative particle dynamics simulations on polymer sheets successfully illustrate spontaneous changes to the tubular and filled scrolls and offer the possibility of internal cavity control. Concluding remarks appear in section IV.

II. ANISOTROPIC LAYER FORMATION

A. Laterally Grafted Rod−Coil Amphiphiles. Let us first consider the rod−coil amphiphiles. Grafted rod−coil molecules (GRCs) have been designed to construct a wide variety of complex geometries.[1,22−24] In particular, T-shaped GRCs (T-GRC) assemble into periodic structures with rod blocks that tend to form long-range ordered structures.[22] Such aggregation behavior of T-GRCs stems from the molecular shape and microphase separation of their structurally inconsistent building blocks. Recently, a penta-*p*-phenylene-conjugated-rod connected to a poly(propylene oxide) (PPO) coil laterally attached through an imidazole linkage (H-GRC) was reported to form tubular scrolls in bulk without the requirement for molecular structure-guiding templates or a selective solvent.[1] While T-GRC and H-GRC have almost identical molecular structures except for the N−H group that is replaced by oxygen, as shown in Scheme 1, only H-GRCs form scrolls by the rolling up of preformed anisotropic 2D layers. In the literature, Brownian dynamics simulations were performed on H-GRC sheet models that are grafted with volume-asymmetric attractive PPO coils.[1] However, the authors did not discuss why H-GRCs conform bilayers in which the coil volume, i.e., the H-GRC density, should differ with respect to the surface side. In addition, the rolling of the sheet models was invoked by the attractive force between the surface grafts. H-GRC layers in bulk are surrounded by other layers whose surface is also covered with PPO coils such that the attractive PPO coils should result in the lamellar phase rather than the scrolls.

To elucidate the underlying mechanism of anisotropic bilayer formation, we scrutinize the intermolecular interaction involved in the self-assembly. T-GRC assembly is governed by the two types of interactions: aromatic rods stack side-by-side[22] or stepwise[25] to maximize the $\pi-\pi$ interaction, whereas bulky PPO coils repel each other leading to energy-minimized structures with long-range ordered rod alignments and the least contact between coils. As a result, where bilayer structures are formed, the surface grafts on both surfaces have well-ordered hexagonal configurations and the bilayer is isotropic overall. H-GRCs can form H-bonds in addition to the $\pi-\pi$ stacking.

The optimized H-GRC dimer structures in Figure 1 and single-point energies in Table 1 were obtained using density

Table 1. Optimized H-GRC[n = 2] and T-GRC[n = 2] Dimers[a]

system		distance[b] (Å)	ΔE[c] (kJ/mol)	ΔE_H (kJ/mol)
H-GRC	H	1.890 [1.883]	−60.660 [−89.952]	−32.926 [−33.294]
	X	2.883 [2.873]		
T-GRC	H	4.633 [4.410]	−27.733 [−56.658]	
	X	5.583 [5.403]		

[a]In gas phase [in diethyl ether solution]. [b]N···H for H-GRC and N···O for T-GRC. [c]$\Delta E = E(H) - E(X)$.

functional theory (DFT).[26] DFT is one of the most widely used quantum calculation methods in diverse fields since it can handle many-body problems to a sufficiently high accuracy whereas it is quite simple to use comparing with Hartree−Fock (HF) method.[27,28] Over the past 40 years, the exchange-correlation functional, the approximated part of the Schrödinger equation, has been developed and improved. To reflect the effect of H-bond upon orientation of GRC molecules, we employed M06-HF/6-311G**++ of Jaguar program[30] M06-HF functional has been developed by Zhao and co-workers specifically targeting to correctly describe weak intermolecular interactions.[29] It is based upon the M06 functional in which empirical parameters from databases are included to overcome several shortcomings of existing exchange-correlational func-

dx.doi.org/10.1021/jp4015564 | J. Phys. Chem. B 2013, 117, 7763−7770

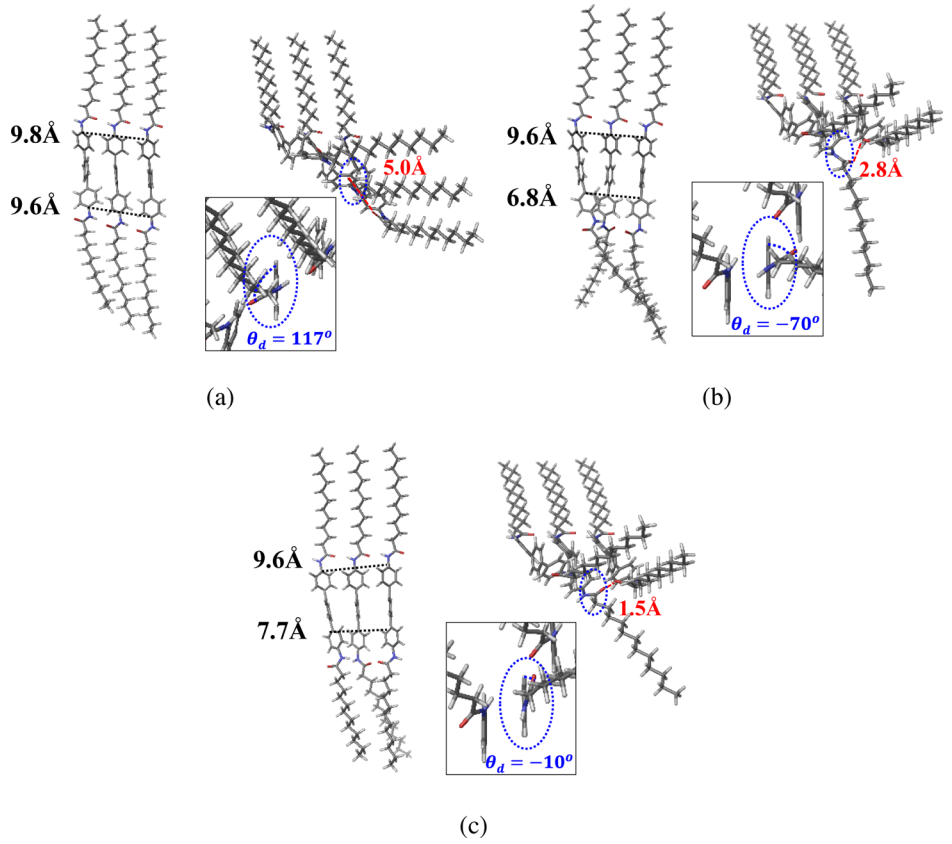

Figure 2. Optimized geometries (top and side views) of L-GRC trimer at (a) an isotropic (both end H-bonded) and (b) an anisotropic (partially H-bonded) configurations. Geometry in (c) represents the energy barrier for the middle coil rotation. The rod−rod distance, the dihedral angle of the benzene ring and the acetamido group, $\theta_d = \angle$[C−C−N−C], and the oxygen−oxygen distances are denoted.

tionals such as B3LYP. In addition to M06 exchange-correlation functional, the full portion of nonlocal HF exchange is included into the exchange-correlation functional. In other words, the M06-HF functional was chosen to study properties of systems in which long-range interactions such as H-bond and $\pi-\pi$ stacking are important.

Diethyl ether solvent was chosen to mimic the PPO coils of neighboring molecules; however, the geometries and energies in the gas phase and diethyl ether lack visible differences. Hereafter, we will refer to the optimized geometry of the H-bonded H-GRC dimer as the H orientation. We also computed H-GRC dimers with the constraint of d[N···H] ≈ 2.9 Å as in Figure 1b, to model the configuration where the N···H distance is too far to form H-bonds, hereafter, the X orientation. Energy stabilization due to H-bond formation, ΔE_H, can be estimated when all other interactions are excluded. Thus, we also performed computations on the T-GRC dimers: single-point energies at the H and X orientations were evaluated for which optimized H-GRC dimer geometries were adapted excluding the oxygen atoms. As in Table 1, $\Delta E_H = [E(H) - E(X)]_{H\text{-}GRC} - [E(H) - E(X)]_{T\text{-}GRC} \approx 33$ kJ/mol, which indicates a strong interaction relative to the weak $\pi-\pi$ stacking.[31]

However, H-bonds induce frustration on the surface graft of the H-GRC bilayer because of the molecular geometry in the H orientation. Frustration is often caused by competing interactions due to site disorder or spin interactions.[32,33] Site disorder in H-GRCs arises because the H-bond length is short: when an H-bond forms, not only imidazole linkages but also the bulky PPO coils approach one another, which produces a large steric effect. Hence the stabilization of the H-bonds and the coil repulsion conflict. In addition, the asymmetric ring structure of the imidazole linkage, the directionality of the H-bonds, and the rigidity of the molecule lead to spinlike frustration at short distances. Spinlike frustration due to the directionality of the H-bonds induces more severe frustration on the layer than the site disorder. H-bonds form only when neighboring molecules acquire a coincident relative orientation, corresponding to the H orientation. Thus, molecules in other orientations should rotate or translate in the plane to take advantage of the stabilization due to H-bonds. The movement of rods, however, is severely hindered because of the $\pi-\pi$ interactions between neighboring rods giving rise to the energy landscape resembling that of glassy systems. Consequently, the coil configuration in H-GRC layers adopts a large number of kinetically trapped local minimum structures similar to amorphous glassy structures.[34] In other words, graft configuration of the two bilayer surfaces is likely to have different H-bonding fractions such that the bilayer is anisotropic overall. Even when the H-bonding fractions of the two surfaces are accidently equal or close, the surface graft configuration will differ and their discrepancy will be sufficient to cause layer anisotropy.[20] Subsequently, the anisotropic bilayer spontaneously transforms into a scroll in agreement with the experiment[1] and, thus, the FAIR mechanism is successfully demonstrated.

B. Linearly Grafted Nonamphiphilic Rod−Coil Molecules. The curve-forming tendency of H-bonding GRCs is irrelevant to amphiphilicity and the location of junction. The nonamphiphilic both end (linearly) grafted rod−coil molecule, *p*-terphenylen-1,4″-ylenebis(dodecanamide) (L-GRC, Scheme

dx.doi.org/10.1021/jp4015564 | J. Phys. Chem. B 2013, 117, 7763−7770

Table 2. Relative Energies of the Isotropic and Anisotropic L-GRC Trimer Configurations

anisotropic	θ_d (deg)	−100	−90	−80	−70	−60	−50	−40
	E (E_h)	.005861	.003485	.001262	0	.003776	.022948	.077443
isotropic	θ_d (deg)	87	97	107	117	127	137	147
	E (E_h)	.689458	.133505	.006430	0	.002318	.006653	.010902

1c), was observed to form a rolled-up organic nanotube from its nanosheet precursor in aqueous solution.[2] As L-GRC aggregate into a single polymer layer, there exist two independent H-bonded surfaces. However, initial aggregation driven by $\pi-\pi$ interaction does not always bring molecules to the orientation where H-bonds can form simultaneously at both junctions. Figure 2 compares the optimized trimer geometries consisting of an isotropic (completely H-bonded surface grafts on both sides) and an anisotropic (partially H-bonded) surface. Energy difference between the (a) and (b) geometries in Figure 2 is 65.9 kJ/mol, qualitatively representing energy stabilization by two H-bonds. More importantly, the distance between rods depends on H-bonding scheme: while the distance is nearly constant (9.6−9.8 Å) at the H-bonded junction, it reduces to 6.8 Å in the absence of H-bonds, i.e., roughly 1.5 Å decrease per missing H-bond, causing substantial discrepancy in the surface area. In addition, owing to the rigidity and the packing geometry within the aggregates, it takes a large amount of energy and time to overcome kinetically trapped barriers and to attain the isotropic layer. To estimate the barrier height for the coil rotation, energies were evaluated as scanning the dihedral angle between the neighboring benzene and the acetamido group, θ_d, of the middle L-GRC from 117° (Figure 2a) to −70° (Figure 2b). The energy difference is listed in Table 2 as a function of θ_d. The largest energy difference was about 650 kJ/mol at $\theta_d = -10°$ (Figure 2c). This indicates that, whereas anisotropic surfaces are metastable, the conversion into isotropic surfaces is kinetically unfavorable. In accordance with the FAIR mechanism, L-GRC layers remain anisotropic on account of disordered partial H-bonding scheme and transform into curved structures.

III. SPONTANEOUS TRANSFORMATION INTO NANOTUBES

Spontaneous scroll transformation of partially H-bonded layers was also investigated using dissipative particle dynamics (DPD) simulations.[35,36] For simplicity, the model sheets were chosen to mimic the H-GRC layers. The partially H-bonded anisotropic sheets were prepared as follows. The reference side was constructed so that coils are grafted in a hexagonal configuration. For the partially H-bonded side, a given fraction (χ_H) of coils is placed next to the neighboring graft to mimic the H-bonds. Note that the graft densities of the two sides are equal. While the other properties of the repulsive coils are exactly identical regardless of the surface side, the locally crowded H-bonded grafts impose a large entropic repulsion on the H-bonded side, causing the flat sheet to be curved. Model sheets were prepared by arranging the coarse-grained rod−coil molecules of 1:1 volume ratio: the rods were arranged parallel to each other so that the sheet surface was grafted with flexible tether coils. Interactions between any two types of rod (R), coil (C), and solvent (S) beads can be described by the soft repulsion in which the parameter $a_{\alpha\beta}$ (α, β = R,C,S) represents the repulsion strength; $a_{\alpha\alpha}$ represents a homogeneous interaction between beads of the same type and is set at $a_{\alpha\alpha} = 25k_BT$,[36] while $a_{\alpha\beta}$ ($\alpha \neq \beta$) represents a heterogeneous interaction between different types of molecular units.[1] The theta solvent condition of the coil beads ($a_{CS} = 25k_BT$) was applied to model the contact between the surface tethers and those on neighboring layers in the solid state.[37] The total number of beads in the simulation box was 675 000 (number density of the system, $\rho = 3$), including solvent beads. All simulations were performed using the time step $\Delta t = 0.02\tau$ at temperature $T = 0.3$. A periodic boundary condition was applied in all directions of the simulation box using the DPD codes in the LAMMPS package.[38] Simulation parameters are listed in Table 3, and the DPD method and simulation details can be found in the literature.[35,36]

Table 3. DPD Potential Parameters[a]

tether coil					sheet					
$a_{\alpha\alpha}$[b]	a_{CS}[b]	a_{RC}[b]	k_{coil}[c]	$\bar{r}_{coil}$[c]	a_{RS}[b]	k_{lat}[c]	k_{long}[c]	$\bar{r}_{lat}$[c]	$\bar{r}_{long}$[c]	k_{ang}[d]
25	25	30	25	0.5	30	100	50	0.5	0.5	20

[a]The subscripts, C, R, and S denote tether coil, sheet (rod), and solvent beads, respectively. $a_{\alpha\beta}$ is in units of k_BT, and the others are in DPD reduced units. [b]DPD repulsion parameter. [c]Harmonic bonding, $V_{bond}(r) = {}^1/_2 k_{bond}(r - \bar{r}_{bond})^2$. [d]Soft angle constraint, $V_{ang}(\theta) = k_{ang}(1 + \cos\theta)$.

Figure 3a−c describes the progress of curvature formation. As the sheet bends, the average distance between the last coil beads, $d_{cc,L}$, increases on the H-bonded surface whereas the distance decreases on the reference side. $d_{cc,F}$ for the first beads varies relatively little compared to $d_{cc,L}$ because they are bound to the sheet. Figure 3d presents the relationship between χ_H and the curvature in terms of $\Delta d_{cc} = \langle d_{cc,L}\rangle - \langle d_{cc,F}\rangle$, where $\langle\ \rangle$ denotes the time average of d_{cc}, which represents the contraction of reference coils (negative sign) and the expansion of H-bonded coils (positive sign). The schematics describe the sheet deformation due to the entropic repulsion caused by the proximity of repulsive coil chains.

In Figure 4, the radius of gyration, $\tilde{R}_g$, and the standard deviation were evaluated from four independent disordered graft configurations at a given χ_H. The radius of gyration was evaluated as

$$\tilde{R}_g = \sqrt{\bar{R}_{xx}^{\ 2} + \bar{R}_{yy}^{\ 2} + \bar{R}_{zz}^{\ 2}} \quad (1)$$

where $\bar{R}_{\alpha\alpha}(\alpha=x,y,z)$ denotes the time evolution of the three principal radii of gyration obtained from the radius of gyration tensor. Its elements are

$$R_{\gamma\delta} = \frac{1}{N_{sheet}} \sum_{i=1}^{N_{sheet}} (\gamma_i - \gamma_{CM})(\delta_i - \delta_{CM}) \quad (2)$$

where γ_i and δ_i are the x, y, and z coordinate of ith bead of the sheet and γ_{CM} and δ_{CM} are those of the center of mass of a sheet consisting of N_{sheet} beads. The magnitude of $\tilde{R}_g$ effectively demonstrates polymer sheet curvature at a given time: large $\tilde{R}_g$ means a slightly curved sheet while small $\tilde{R}_g(t)$ describes a large curved or scrolled structure. The larger χ_H induces a higher curvature (smaller $\tilde{R}_g$) as a result of the increased coil repulsion,

dx.doi.org/10.1021/jp4015564 | J. Phys. Chem. B 2013, 117, 7763−7770

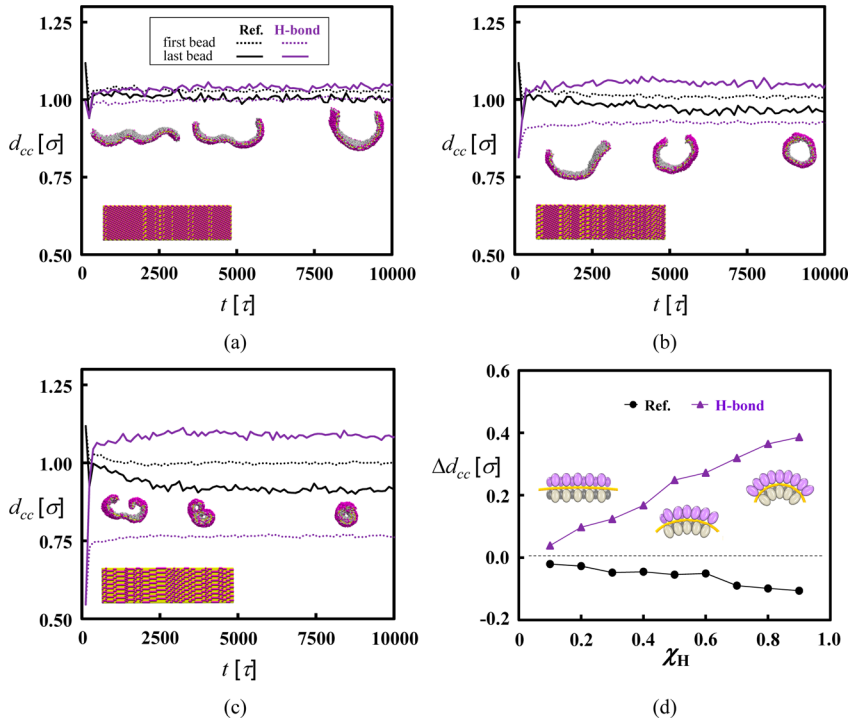

Figure 3. Time evolution of the average nearest coil−coil distances (d_{cc}) between, respectively, first beads (dotted lines) and last beads (solid lines) at the relative H-bonding fraction, (a) χ_H = 0.1, (b) 0.3, and (c) 0.7. Partially H-bonded surface grafts are also shown at the lower left corner. In (d), relationship between χ_H and Δd_{cc} is illustrated with schematic pictures of curved sheets.

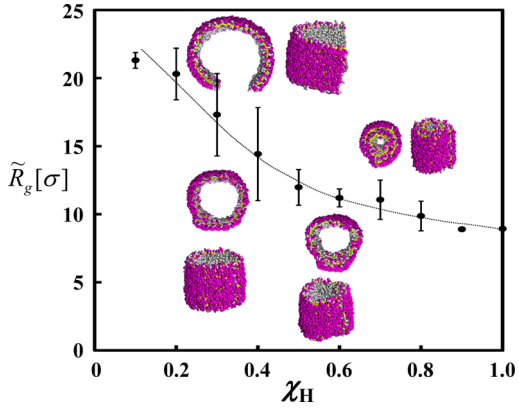

Figure 4. Relationship between the relative fraction of H-bonds (χ_H) and the radius of gyration ($\tilde{R}_g$).

suggesting that the size of the internal cavity is closely associated with χ_H. In practice, both composing layers are frustrated with fractional H-bonding, and thus, the relative fraction of H-bonds between the two surfaces is expected to be small but not negligible. When a longer sheet was used, differences no greater than χ_H = 0.1 will result in tubular scrolls.

In addition, the curvature (κ) and the internal cavity diameter (D_{inner}), respectively, are presented in Figure 5, a and b. In general, the curvature, κ, is calculated for a parametrically defined space curve in three dimensions as

$$\kappa = \frac{\sqrt{(x''y' - y''x')^2 + (x''z' - z''x')^2 + (y''z' - z''y')^2}}{(x'^2 + y'^2 + z'^2)^{3/2}} \quad (3)$$

Since the polymer sheet always scrolls along the longitudinal direction having lateral side as the length of the tubes, a two-dimensional analogue of eq 3 was used to evaluate the curvature and the internal cavity diameter as

$$\kappa_{plane} = \frac{|x'y'' - y'x''|}{(x'^2 + y'^2)^{3/2}} \quad (4)$$

To obtain the two-dimensional curve fit, we first defined a tubule vector, which is parallel to the tubule direction, by connecting the centers of mass of the first and the last 10 rows of layer beads. After defining the tubule vector, we rotated the tube such that its tubule vector aligns with the z-axis. After the rotation, we projected the middle layer beads onto the xy-plane as shown in Figure 6 and fitted to a circle. The plane curvature is then evaluated using eq 4 based on the fitted circle.

Figure 5 shows that the curvature exhibits a linear dependence, whereas the internal cavity diameter shows a power law relationship with respect to χ_H. According to Figure 5b, one can expect a value of $D_{inner} > 12\sigma$ in the DPD length unit for $\chi_H < 0.1$. Considering the volume of the H-GRC, $D_{inner} > 12\sigma$ is equivalent to an internal cavity diameter of $D_{inner} > 119_{nm}$. In the literature,[1] H-GRC[n=15] formed tubular scrolls with an internal cavity diameter of approximately 30 nm. The coil's volume fraction in H-GRC[n=15] was estimated to be $f_V \approx 0.8$, but $f_V = 0.5$ for the model considered here. In this case, the dimension roughly corresponds to H-GRC[n=8]. As the coil volume fraction increases, the internal cavity diameter also increases because of the large coil entropy.[19] Hence, the internal cavity of H-GRC[n=15] is larger than what is estimated for H-GRC[n=8].

The strong correlation of $\tilde{R}_g$, κ, and D_{inner} with the degree of layer anisotropy also implies that the internal cavity size of nanotubes can be systematically controlled by carefully regulating the H-bonding fraction and/or scheme. As the nonamphiphilic building blocks such as L-GRCs assemble in

dx.doi.org/10.1021/jp4015564 | J. Phys. Chem. B 2013, 117, 7763−7770

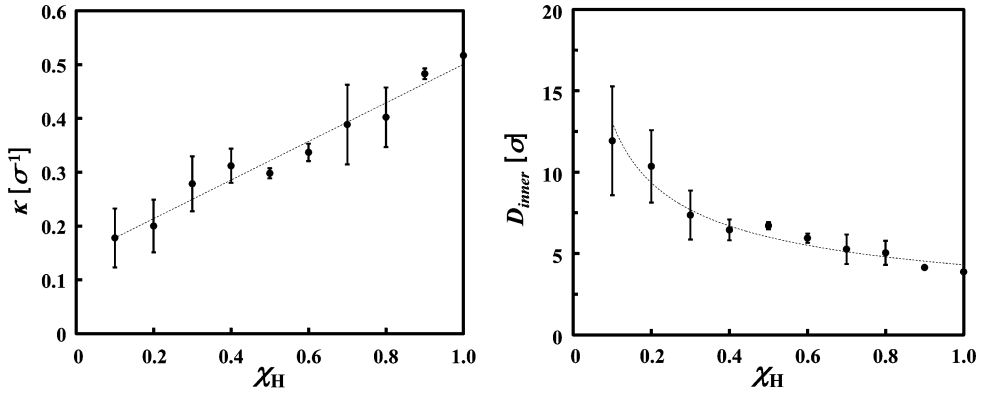

(a) (b)

Figure 5. Relationship between the relative fraction of H-bonds (χ_H) and (a) the curvature (κ) and (b) the internal cavity diameter (D_{inner}).

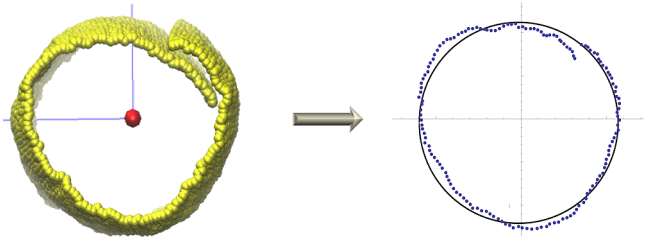

(a) (b)

Figure 6. (a) Top view of a tube and (b) its orthogonal projected plane curve. In (a), the two (overlapped) red beads represent the center of mass that define the tubule vector. Yellow beads are the layer beads while surface coils are eliminated for clarity. In (b) blue dots stand for the projected positions of the middle layer beads.

aqueous solution, the layer bonding scheme becomes more amorphous because H_2O-participated H-bonds[39] disturb the already unstable bonding scheme and allow a greater degree of layer anisotropy. Therefore, curvature of the layer is expected to increase with water content, which explains the concentration-dependent curvature observed in experiments: the lower the complex concentration, the higher the curvature of the self-assembled architecture.[2,3] Once nanotubes are formed, the nanotubes can be stored for a long period of time upon drying because molecular rearrangement is suppressed due to the strong intermolecular interaction in bulk. For the reason, though it may take up to several days, organic solvents unwind nanotubes into layered sheets.[2] Organic solvent molecules readily penetrate into the hydrophobic polymer layer, loosen the intermolecular interaction, and, thus, help molecules to rearrange until they reach isotropic surfaces. The opposite may occur to the H-GRC nanotubes. The nanotubes in bulk are anticipated to turn into lamellar in the presence of water as the imidazole linkages preferentially form H-bonds with water molecules, eliminating the conflict between molecular interactions. Such a reversible transformation is worth examining for the purpose of curvature control. By manipulating solvent composition and using the freezing−drying method, one should be able to control the internal cavity size of the rigid organic nanotubes.

IV. CONCLUDING REMARKS

In this work, the FAIR mechanism for anisotropic higher-order architecture formation was proposed and demonstrated for H-bond-driven rigid nanotube formation. Initially, molecular aggregation occurs and polymer sheets form due to microphase separation driven by intermolecular interactions such as $\pi-\pi$ stacking or amphiphilicity. Such interactions are neither selective nor directional; hence, the aggregates lack long-range orders in microscopic molecular configuration. After the layer formation, intermolecular H-bonds begin to form depending on their relative orientations. Obviously, not all molecules have the right orientation to form H-bonds for additional stability. Flexible molecules are relatively free to rearrange themselves within the aggregate and form H-bonds. In contrast, rearrangement of the building blocks with rigid segments requires collective and cooperative motion which demands a large amount of energy to overcome the interaction among the network of molecules. The combination of H-bonds and rigid molecular geometry prevents or delays the layer from attaining the well-ordered arrangement. Consequently, self-assembled layers have inhomogeneous H-bonding scheme at various fractions giving rise to a layer that is anisotropic overall and that undergoes spontaneous transformation into curved structures including nanotubes, scrolls, vesicles, etc.

H-bond-driven nanotube formation is not limited to the rod−coil molecules. In fact, the FAIR mechanism is applicable to any building blocks as long as the rigid moiety inhibits directional intermolecular interaction. In the recent literature, the self-assembled nonamphiphilic β-cyclodextrin/ionic surfactant (β-CD/IS) complexes form annular ringlike nanotubes and vesicles in aqueous solution.[3] Although further information should be supported by experimental and theoretical investigations, the FAIR mechanism driven by the frustrated H-bonding scheme might have caused the nanotube formation of CD/IS complexes. By comparing the self-assembly of β-CD/IS with that of α-CD/IS, with which nanotube formations have not been seen, the influence of the molecular geometry on anisotropic layer formation becomes apparent. β-CD has heptagon shape and readily forms host−guest complexes by the inclusion of IS, whereas α-CD is its hexagonal analogue. As they form bilayers, hexagonal α-CD/IS easily attains the long-range order on both layers with the complete H-bonding scheme. On the other hand, the asymmetrical geometry of β-CD/IS prohibits the bond formation of the seven H-bonding

dx.doi.org/10.1021/jp4015564 | J. Phys. Chem. B 2013, 117, 7763−7770

sites. It suggests that there should be various H-bonding schemes, i.e., fractions and configurations, of β-CD/IS layers so that the formed bilayer is thermodynamically metastable and anisotropic leading to nanotube formation. The possibility is currently under investigation in our group.

The introduction of H-bonding into building blocks is simple yet highly versatile. Thus, the H-bond-driven anisotropic layer and curvature formation can make a significant impact on the development of rigid organic nanotubes. In addition, understanding on the frustration-driven anisotropic higher-order structure formation can readily be extended to the self-assembly of hybrid building blocks, regardless of amphiphilicity, such as polymer nanocomposites as long as the rigid moiety of building blocks conflicts with the directionality of H-bonds.

AUTHOR INFORMATION

Corresponding Author

*E-mail: esim@yonsei.ac.kr.

Notes

The authors declare no competing financial interest.

ACKNOWLEDGMENTS

We acknowledge the financial support from the Ministry of Education, Science and Technology through the national research foundation (NRF) grant (2010-220-C00017 and 2012R1A1A2004782) and the project EDISON (2012M3C1A6035358). M.H. and J.H. thank the fellowship of the BK 21 program from MOEHRD.

REFERENCES

(1) Hong, D.-J.; Lee, E.; Jeong, H.; Lee, J.-k.; Zin, W.-C.; Nguyen, T. D.; Glotzer, S. C.; Lee, M. Solid-State Scrolls from Hierarchical Self-Assembly of T-Shaped Rod−Coil Molecules. *Angew. Chem., Int. Ed.* **2009**, *48*, 1664−1668.

(2) Chen, Y.; Zhu, B.; Zhang, F.; Han, Y.; Bo, Z. Hierarchical Supramolecular Self-Assembly of Nanotubes and Layered Sheets. *Angew. Chem.* **2008**, *120*, 6104−6107.

(3) Jiang, L.; Peng, Y.; Yan, Y.; Deng, M.; Wang, Y.; Huang, J. "Annular Ring" Microtubes Formed by SDS@2β-CD Complexes in Aqueous Solution. *Soft Matter* **2010**, *6*, 1731−1736.

(4) Park, C.; Lee, I. H.; Lee, S.; Song, Y.; Rhue, M.; Kim, C. Cyclodextrin-covered organic nanotubes derived from self-assembly of dendrons and their supramolecular transformation. *Proc. Natl. Acad. Sci. U.S.A.* **2006**, *103*, 1199−1203.

(5) Luo, S.-C.; Sekine, J.; Zhu, B.; Zhao, H.; Nakao, A.; Yu, H.-h. Polydioxythiophene Nanodots, Nonowires, Nano-Networks, and Tubular Structures: The Effect of Functional Groups and Temperature in Template-Free Electropolymerization. *ACS Nano* **2012**, *6*, 3018−3026.

(6) Mes, T.; Koenigs, M. M. E.; Scalfani, V. F.; Bailey, T. S.; Meijer, E. W.; Palmans, A. R. A. Network Formation in an Orthogonally Self-Assembling System. *ACS Macro Lett.* **2011**, *1*, 105−109.

(7) Guo, C. F.; Zhang, J.; Tian, Y.; Liu, Q. A General Strategy to Superstructured Networks and Nested Self-Similar Networks of Bismuth Compounds. *ACS Nano* **2012**, *6*, 8746−8752.

(8) Cölfen, H.; Mann, S. Higher-Order Organization by Mesoscale Self-Assembly and Transformation of Hybrid Nanostructures. *Angew. Chem., Int. Ed.* **2003**, *42*, 2350−2365.

(9) Che, G.; Lakshmi, B. B.; Fisher, E. R.; Martin, C. R. Carbon nanotubule membranes for electrochemical energy storage and production. *Nature* **1998**, *393*, 346−349.

(10) Kowalczyk, P.; Solarz, L.; Do, D. D.; Samborski, A.; MacElroy, J. M. D. Nanoscale Tubular Vessels for Storage of Methane at Ambient Temperatures. *Langmuir* **2006**, *22*, 9035−9040.

(11) Karlsson, A.; Karlsson, R.; Karlsson, M.; Cans, A.-S.; Stromberg, A.; Ryttsen, F.; Orwar, O. Molecular engineering: Networks of nanotubes and containers. *Nature* **2001**, *409*, 150−152.

(12) Son, S. J.; Bai, X.; Nan, A.; Ghandehari, H.; Lee, S. B. Template synthesis of multifunctional nanotubes for controlled release. *J. Controlled Release* **2006**, *114*, 143−152.

(13) Shimizu, T.; Masuda, M.; Minamikawa, H. Supramolecular Nanotube Architectures Based on Amphiphilic Molecules. *Chem. Rev. (Washington, DC, U.S.)* **2005**, *105*, 1401−1444.

(14) Stone, D. A.; Tayi, A. S.; Goldberger, J. E.; Palmer, L. C.; Stupp, S. I. Self-assembly and conductivity of hydrogen-bonded oligothiophene nanofiber networks. *Chem. Commun. (Cambridge, U.K.)* **2011**, *47*, 5702−5704.

(15) Bushey, M. L.; Nguyen, T.-Q.; Zhang, W.; Horoszewski, D.; Nuckolls, C. Using Hydrogen Bonds to Direct the Assembly of Crowded Aromatics. *Angew. Chem., Int. Ed.* **2004**, *43*, 5446−5453.

(16) Jana, P.; Maity, S.; Maity, S. K.; Ghorai, P. K.; Haldar, D. Insights into H-aggregates and CHO hydrogen bond mediated self-assembly of pyromellitic bisimide. *CrystEngComm* **2012**, *14*, 6586−6592.

(17) Knauert, S. T.; Douglas, J. F.; Starr, F. W. Morphology and Transport Properties of Two-Dimensional Sheet Polymers. *Macromolecules* **2010**, *43*, 3438−3445.

(18) Radzihovsky, L.; Toner, J. A New Phase of Tethered Membranes: Tubules. *Phys. Rev. Lett.* **1995**, *75*, 4752−4755.

(19) Han, M.; Sim, E. Formation of Tubular Scrolls with Controlled Internal Cavity. *J. Phys. Chem. B* **2012**, *116*, 1796−1801.

(20) Han, M.; Sim, E. Surface Graft Configuration Dependency of the Morphologies of Heterosurface Sheet Polymers. *J. Phys. Chem. B* **2012**, *116*, 5771−5776.

(21) Sadoc, J.-F.; Mosseri, R. *Geometrical Frustration*; Cambridge University Press: Cambridge, UK, 1999.

(22) Horsch, M. A.; Zhang, Z.; Glotzer, S. C. Self-Assembly of Laterally-Tethered Nanorods. *Nano Lett.* **2006**, *6*, 2406−2413.

(23) Liu, L.; Hong, D.-J.; Lee, M. Chiral Assembly from Achiral Rod−Coil Molecules Triggered by Compression at the Air−Water Interface. *Langmuir* **2009**, *25*, 5061−5067.

(24) He, L.; Zhang, L.; Ye, Y.; Liang, H. Solvent-Induced Self-Assembly of Polymer-Tethered Nanorods. *J. Phys. Chem. B* **2010**, *114*, 7189−7200.

(25) Hong, D.-J.; Lee, E.; Lee, J.-K.; Zin, W.-C.; Han, M.; Sim, E.; Lee, M. Stepped Strips from Self-Organization of Oligo(p-Phenylene) Rods with Lateral Dendritic Chains. *J. Am. Chem. Soc.* **2008**, *130*, 14448−14449.

(26) Parr, R. G.; Yang, W. *Density-functional Theory of Atoms and Molecules*; Oxford University Press: New York, 1994.

(27) Hohenberg, P.; Kohn, W. Inhomogeneous Electron Gas. *Phys. Rev.* **1964**, *136*, B864−B871.

(28) Kohn, W.; Sham, L. J. Self-Consistent Equations Including Exchange and Correlation Effects. *Phys. Rev.* **1965**, *140*, A1133−A1138.

(29) Zhao, Y.; Truhlar, D. G. Density Functional for Spectroscopy: No Long-Range Self-Interaction Error, Good Performance for Rydberg and Charge-Transfer States, and Better Performance on Average than B3LYP for Ground States. *J. Phys. Chem. A* **2006**, *110*, 13126−13130.

(30) *Jaguar 7.7*; Schrodinger, LLC: New York, 2010.

(31) Steed, J. W.; Atwood, J. L. *Supramolecular Chemistry*; Wiley: Chichester, UK, 2009.

(32) Villain, J. Spin Glass with Non-Random Interactions. *J. Phys. C: Solid State* **1977**, *10*, 1717.

(33) Ruderman, M. A.; Kittel, C. Indirect Exchange Coupling of Nuclear Magnetic Moments by Conduction Electrons. *Phys. Rev.* **1954**, *96*, 99−102.

(34) Zallen, R. *The Physics of Amorphous Solids*; John Wiley & Sons: Weinheim, Germany, 1998.

(35) Español, P.; Warren, P. Statistical Mechanics of Dissipative Particle Dynamics. *Europhys. Lett.* **1995**, *30*, 191−196.

(36) Groot, R. D.; Warren, P. B. Dissipative Particle Dynamics: Bridging the Gap Between Atomistic and Mesoscopic Simulation. *J. Chem. Phys.* **1997**, *107*, 4423−4435.
(37) Gedde, U. W. *Polymer physics*; Chapman & Hall: London, 1995.
(38) http://lammps.sandia.gov.
(39) Di Blasio, B.; Galdiero, S.; Saviano, M.; Pedone, C.; Benedetti, E.; Rizzarelli, E.; Pedotti, S.; Vecchio, G.; Gibbons, W. A. Synthesis and structural characterization of 6I,6II-diamino-6I,6II-dideoxy-cyclomaltoheptaose, a difunctionalized β-cyclodextrin. *Carbohydr. Res.* **1996**, *282*, 41−52.